# REPORT DOCUMENTATION PAGE

*Form Approved*
*OMB No. 0704-0188*



| **1. REPORT DATE** *(DD-MM-YYYY)* | **2. REPORT TYPE** | **3. DATES COVERED** *(From - To)* |
|---|---|---|
| 15-11-2010 | Technical Paper | |

**4. TITLE AND SUBTITLE**

**Laser-Induced Fluorescence Velocity Measurements of a Diverging Cusped Field Thruster**

**5a. CONTRACT NUMBER**

**5b. GRANT NUMBER**

**5c. PROGRAM ELEMENT NUMBER**

**6. AUTHOR(S)**
Natalia A. MacDonald & Mark A. Cappelli (Stanford)
Stephen R. Gildea & Manuel Martinez-Sanchez (MIT)
William A. Hargus, Jr. (AFRL/RZSS)

**5d. PROJECT NUMBER**

**5e. TASK NUMBER**

**5f. WORK UNIT NUMBER**
**23080535**

**7. PERFORMING ORGANIZATION NAME(S) AND ADDRESS(ES)**

Stanford University
Stanford Plasma Physics Laboratory
Stanford, CA 94305

**8. PERFORMING ORGANIZATION REPORT NUMBER**

AFRL-RZ-ED-TP-2010-500

**9. SPONSORING / MONITORING AGENCY NAME(S) AND ADDRESS(ES)**

Air Force Research Laboratory (AFMC)
AFRL/RZS
5 Pollux Drive
Edwards AFB CA 93524-7048

**10. SPONSOR/MONITOR'S ACRONYM(S)**

**11. SPONSOR/MONITOR'S NUMBER(S)**
AFRL-RZ-ED-TP-2010-500

**12. DISTRIBUTION / AVAILABILITY STATEMENT**

Approved for public release; distribution unlimited (PA #10593).

**13. SUPPLEMENTARY NOTES**
For presentation at the 47th AIAA/ASME/ASEE Joint Propulsion Conference, San Diego, CA, 31 Jul-03 Aug 2011.

**14. ABSTRACT**

Measurements are presented of the most probable time-averaged ion velocities within the acceleration channel and in the plume of a diverging cusped field thruster operating on xenon. Xenon ion velocities for the thruster are derived from laser-induced fluorescence measurements of the 5*d*[4]7/2 − 6*p*[3]5/2 xenon ion excited state transition centered at _ = 834.72 nm. The thruster is operated in both a high current mode, where the anode discharge current is shown to oscillate periodically, and a low current mode where operation is relatively quiescent. In the low current mode, ion emission is predominantly in the form of a conical jet, whereas in the high current mode, the emission is still divergent but more diffuse througout the cone angle. The diffuse plume may be related to the oscillatory nature of the high current mode, where the regions of ionization and ion acceleration may oscillate between the second and third outer cusps in the channel.

**15. SUBJECT TERMS**

| **16. SECURITY CLASSIFICATION OF:** | | | **17. LIMITATION OF ABSTRACT** | **18. NUMBER OF PAGES** | **19a. NAME OF RESPONSIBLE PERSON** |
|---|---|---|---|---|---|
| | | | | | Dr. William A. Hargus, Jr. |
| **a. REPORT** | **b. ABSTRACT** | **c. THIS PAGE** | SAR | 15 | **19b. TELEPHONE NUMBER** *(include area code)* |
| **Unclassified** | **Unclassified** | **Unclassified** | | | N/A |

# Laser-Induced Fluorescence Velocity Measurements of a Diverging Cusped Field Thruster

Natalia A. MacDonald and Mark A. Cappelli
*Stanford Plasma Physics Laboratory*
*Stanford University*
*Stanford, CA 94305*

Stephen R. Gildea and Manuel Martínez-Sánchez
*Space Propulsion Laboratory*
*Massachusetts Institute of Technology*
*Cambridge, MA 02139*

William A. Hargus, Jr.
*Spacecraft Propulsion Branch*
*Air Force Research Laboratory*
*Edwards AFB, CA 93524*

**Measurements are presented of the most probable time-averaged ion velocities within the acceleration channel and in the plume of a diverging cusped field thruster operating on xenon. Xenon ion velocities for the thruster are derived from laser-induced fluorescence measurements of the $5d[4]_{7/2} - 6p[3]_{5/2}$ xenon ion excited state transition centered at $\lambda = 834.72$ nm. The thruster is operated in both a high current mode, where the anode discharge current is shown to oscillate periodically, and a low current mode where operation is relatively quiescent. In the low current mode, ion emission is predominantly in the form of a conical jet, whereas in the high current mode, the emission is still divergent but more diffuse througout the cone angle. The diffuse plume may be related to the oscillatory nature of the high current mode, where the regions of ionization and ion acceleration may oscillate between the second and third outer cusps in the channel.**

## I. Introduction

Electric propulsion devices such as Hall thrusters have proven to be an effective alternative to chemical thrusters for applications such as satellite station keeping and primary propulsion systems for deep-space missions.[1] The typical annular Hall thruster employs a crossed radial magnetic field and axial electric field to trap electrons in their channel, ionize propellant and accelerate the ions out of the thruster.[2] A limiting factor for the lifetime of these thrusters is erosion of the electrically insulating channel walls due to heat loading and sputtering from high energy ions.[2,3] To mitigate erosion, several thruster designs incorporating cusped magnetic field profiles that keep high energy ions away from channel walls are currently



American Institute of Aeronautics and Astronautics
Approved for public release; distribution is unlimited.

being studied. These include the High Efficiency Multi-stage Plasma (HEMP) thruster developed by the THALES Research Institute,[4,5] the Princeton University Cylindrical Hall Thruster (CHT),[6–9] the Massachusetts Institute of Technology (MIT) Diverging Cusped Field Thruster (DCFT),[10] and the Stanford University Diverging Cusped Field (DCF) Thruster.[11]

The concept of cusped field thrusters draws from experience with Hall thrusters[6] and traveling wave tubes.[12] Strong magnets of alternating polarity along the thruster channel create cusped magnetic profiles that are largely in the axial direction. Magnetic bottles trap incoming electrons, allowing for effective propellant ionization. A strong radial portion of the magnetic field is seen only at magnet interfaces, thereby minimizing ion bombardment and heat dissipation to the walls.[4] Combined with strong electric field gradients that impede electron movement towards the anode,[4] cusped field thrusters effectively accelerate ions with minimal wall interactions. Recent work on cusped field thrusters has shown that they vary greatly from traditional Hall thrusters.[6,13–18] Cusped field thrusters tend to have a large portion of their ion acceleration outside of the thruster, and a high divergence angle with radial ion velocities of comparable magnitude of axial ion velocities.[14] Unlike Hall thrusters, the strong magnetic fields seen in cusped field designs using permanent magnets ($\approx 0.5$ Tesla)[19] do not rule out the possibility that ions may be weakly magnetized. Therefore, in some regions of these cusped field thrusters there could be a significant ion $\vec{E} \times \vec{B}$ drift.

To further understand the operation of cusped field thrusters, this study seeks to characterize one particular variant, the MIT DCFT, using laser-induced fluorescence (LIF) velocimetry. A survey of the axial velocities within the acceleration channel and axial and radial velocities in the near-field of the plume of the DCFT is presented. The DCFT incorporates permanent magnets of alternating polarity to create the cusped magnetic field profile while reducing thruster weight and power consumption by eliminating the magnetic circuit.[20] It has a diverging, cone shaped channel to further minimize ion bombardment near the exit plane. It also has a hollow, cone-shaped plume[17] where the highest current densities and highest ion velocities appear in a "jet" at an angle of 30° to 40° from the centerline of the thruster.[21]

As described below, time-averaged xenon ion velocities for the thruster are derived from LIF measurements of the $5d[4]_{7/2} - 6p[3]_{5/2}$ xenon ion excited state transition at $\lambda = 834.72$ nm. The measured spectral feature, which is a convolution of the ion velocity distribution function (VDF), and the transition lineshape, is used to determine the most probable velocities at various positions throughout the thruster channel and in the plume. These velocities are used to determine the ion kinetic energies and to estimate electric field strength along the centerline of the thruster.

## II. Experiment

A schematic of the DCFT is shown in Fig. 1.[16] The acceleration channel in the DCFT has a diverging, cone shape that is 49.5 mm in depth, 28 mm in radius at the exit plane, with a cone half angle of 22.5°.[20] Permanent magnets of alternating polarity are placed along the channel with decreasing strength as they approach the exit plane. This results in a magnetic field profile that is largely in the axial direction, with radial components at the magnet interfaces (i.e. cusps). The cusped magnetic fields produce a magnetic bottle effect for incoming electrons, trapping them between cusps where they mirror back and forth, allowing for a high ionization percentage and preventing electrons from the external cathode from traveling directly to the anode. This design is intended to reduce erosion and wall losses by preventing the plasma from hitting the channel walls.

The MIT DCFT tends to operate in either a high current or low current mode. The high current mode is characterized by periodic oscillations in the discharge current, while the low current mode is quiescent, as shown by the anode current traces in Fig. 2. The specifications for the high and low current operating

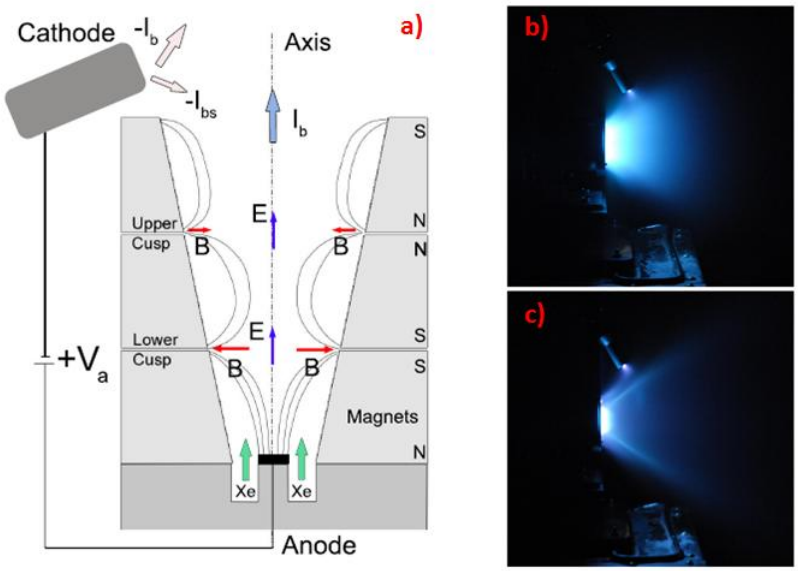


**Figure 1. Diverging Cusped Field Thruster, developed by MIT. a) Schematic of DCFT,[16] b) Operation in high current mode, c) Operation in low current mode.**

conditions examined in this study are given in Tables 1 and 2. The high current mode, achieved by running the thruster with an 830 $\mu g/s$ flow rate and 300 V anode potential, was chosen to match a highly efficient operating condition demonstrated in previous work at MIT[20] while maintaining a power of less than 200 W. The 200 W restriction was imposed to prevent heat loading on the magnets from degrading the magnetic field significantly during long tests.

The second operating condition was chosen to demonstrate the low power mode of operation. Transitioning from high to low current mode can be achieved by either raising the applied anode voltage or by lowering the propellant flow rate to the anode. The first attempt at operating the thruster in the low current mode by raising the voltage to 400 V while maintaining 830 $\mu g/s$ of flow rate proved unsuccessful, as the thruster reverted back to the high current mode within about 30 minutes. To maintain operation in the low current mode while keeping the operating power less than 200 W, it was necessary to both raise the voltage and lower the anode flow rate. The resulting low current operating condition used in this study had an anode potential of 400 V and flow rate of 590 $\mu g/s$. Both conditions were run with a background chamber pressure of $5 \times 10^{-6}$ Torr during thruster operation (corrected for xenon).

In this experiment, LIF is used to measure the most probable velocities of ions in the thruster channel and plume. LIF is a particularly useful diagnostic for electric propulsion devices such as the DCFT where plasmas create harsh, non-uniform environments. It is a spatially resolved measurement and is non-intrusive by nature, as compared to electrostatic probes which physically perturb the operation of the plasma they are trying to measure.

Ion velocity measurements are accomplished by probing the $5d[4]_{7/2} - 6p[3]_{5/2}$ electronic transition of Xe II at 834.72 nm. The upper state of this transition is shared by the relatively strong $6s[2]_{3/2} - 6p[3]_{5/2}$ transition at 541.92 nm,[22] allowing for non-resonant fluorescence collection. Ion velocities are determined by measuring the Doppler shift of the absorbing ions.[23] Benefits of the $5d[4]_{7/2} - 6p[3]_{5/2}$ transition include the ease of accessibility using a cw diode laser, and the option of non-resonant fluorescence collection using the $6s[2]_{3/2} - 6p[3]_{5/2}$ transition which mitigates noise induced by surface reflections of the probe beam.[22,24]

One drawback to this transition is that for the 19 isotopic and spin split components contributing to

the hyperfine structure of the $5d[4]_{7/2} - 6p[3]_{5/2}$ xenon ion transition, only the $6p[3]_{5/2}$ upper state has confirmed nuclear spin splitting constants.[24–27] The hyperfine splitting constants characterize the small variations in state energies associated with the odd-numbered isotopes, which contribute to broadening in the measured spectral feature. This transition was first used by Manzella[28] to make velocity measurements in a Hall thruster plume. In that study, splitting constants for the similar $5d^4D_{7/2} - 6p^4P_{5/2}$ transition at 605.1 nm were used in modeling the transition lineshape, and it was shown that Doppler broadening generally dominates the broadening mechanisms in these type of plasmas. The $5d[4]_{7/2} - 6p[3]_{5/2}$ has since been used throughout the electric propulsion community to characterize a variety of thrusters operating on xenon.[14,29,30]

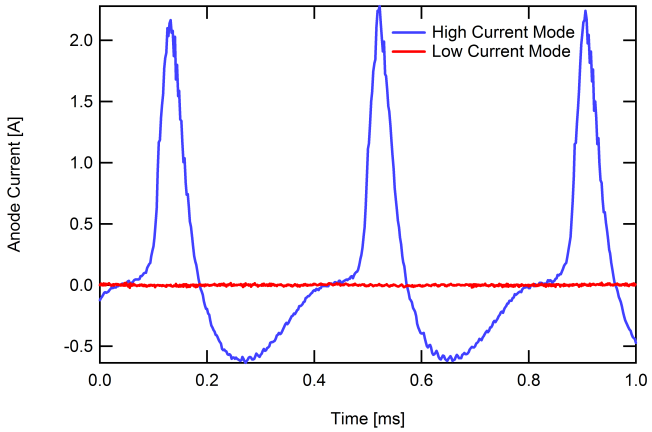


**Figure 2. Anode current traces for high and low current operating conditions. Note: the current probe was AC coupled.**

**Table 1. High current operating condition.**

| | |
|---|---|
| Anode Flow | 830 $\mu g/s$ Xe |
| Cathode Flow | 150 $\mu g/s$ Xe |
| Anode Potential | 300 V |
| Anode Current | 0.53 A |
| Keeper Current | 0.50 A |
| Heater Current | 3.0 A |

**Table 2. Low current operating condition.**

| | |
|---|---|
| Anode Flow | 590 $\mu g/s$Xe |
| Cathode Flow | 150 $\mu g/s$ Xe |
| Anode Potential | 400 V |
| Anode Current | 0.17 A |
| Keeper Current | 0.50 A |
| Heater Current | 3.0 A |

LIF measurements for this study were performed at the Air Force Research Laboratory (AFRL) Electric Propulsion Laboratory at Edwards AFB, CA. This experimental apparatus has been described extensively in previous work.[29,31] Fig. 3 shows a top view of the experimental set-up, including the thruster, one branch of the probe optics and the collection optics. The thruster is mounted on a system of orthogonal translation

stages that allows for three axes of motion. The anode and cathode potentials are floating with respect to ground. The cathode is located to the side of the thruster opposite to the collection optics with the tip at a radial distance of 40 mm from the centerline and axial distance of 28 mm from the exit plane with its axis oriented at an angle of 70° degrees with respect to the outward normal to the exit plane. This is consistent with previous studies.[10,20,21]

The laser is a New Focus Vortex TLB-6017 tunable diode laser, capable of tuning approximately ±50 GHz about a center wavelength of 834.72 nm. The 10 mW beam is passed through several beam pick-offs followed by a 50-50 cube beam splitter where it is split into two beams of equal power, approximately 5 mW each. The axial probe beam, shown in both Figs. 3 and 4, is focused by a lens and enters the vacuum chamber through a window. The radial beam, shown in Fig. 4 only, is periscoped from the optical bench to the top of the chamber such that it enters the chamber from above the thruster and probes the velocity perpendicular to the axial beam. Each probe beam is chopped at a unique frequency by choppers Ch2 (2kHz) and Ch3 (2.8 kHz) for phase sensitive detection of the fluorescence signals.

The two wedge beam splitters (BS) shown in Fig. 3 provide portions of the beam for wavelength and velocity calibration. These include use of a commercial wavelength meter and a 300 MHz free spectral range Fabry-Perot etalon (F-P) to monitor wavelength during a laser scan, and a low pressure xenon hollow cathode discharge lamp to provide a stationary absorption reference for the determination of the unshifted spectral line position (zero velocity reference). The xenon lamp has no detectable population of the ionic xenon $5d[4]_{7/2}$ state, therefore the nearby (estimated to be 18.1 GHz distant) neutral xenon $6s'[1/2]_1 - 6p'[3/2]_2$ transition at 834.68 nm[32,33] is used for the reference.

The fluorescence collection optics are also shown in Fig. 3. The fluorescence is collected by a 75 mm diameter, 300 mm focal length lens within the chamber and oriented 60° from the probe beam axis. The plume divergence half angle of DCFT has previously been measured as 70° for 90% of the integrated beam current. However, the peak ion flux lies between 30° and 40° and drops off by more than 75% by the 70° point.[21] By placing the LIF collection optics at 60° off this axis,[29] it is possible to interrogate points along the centerline up to 20 mm inside the thruster acceleration channel, while keeping the lenses and mirrors away from much of the plume ion flux. In this way, it is possible to probe internal ion acceleration of the DCFT with minimal intrusion into the plume and without destroying the collection optics through sputtering. The collimated fluorescence signal is directed through a window in the chamber side wall to a similar lens that focuses the collected fluorescence onto the entrance slit of the 125 mm focal length monochromator with a photomultiplier tube (PMT) at its exit. Due to the 1:1 magnification of the collection optics, the spatial resolution of the measurements is determined by the geometry of the entrance slit (0.7 mm width and 1.5 mm height) as well as the sub-mm diameter of the probe beam.

The combination of thruster geometry and collection optics allows for a large region of the DCFT channel and plume to be interrogated; however, lower S/N closer to the anode and along the centerline of the plume limit the measurements that are meaningful. The current density along the centerline of the thruster is far less than that seen in the jet between 30° and 40°. For the high current mode, the centerline current density is a factor of two less than that in the jet, while for the low current mode, it is a full order of magnitude less,[21] creating a hollow plume. In this region, the S/N is much lower than in the jet, since the fluorescence signal strength is strongly dependent on the number density of excited ions, $N_2$,[34] i.e.:

$$S_f = \eta_d h\nu_{12} N_2 V A_{21} \frac{\Omega}{4\pi} \tag{1}$$

In this equation, $\eta_d$ is the collection efficiency, $h\nu_{12}$ represents the energy separation between upper and lower states, $V$ is the volume of the intersecting laser and collection optics, $A_{21}$ is the Einstein coefficient for

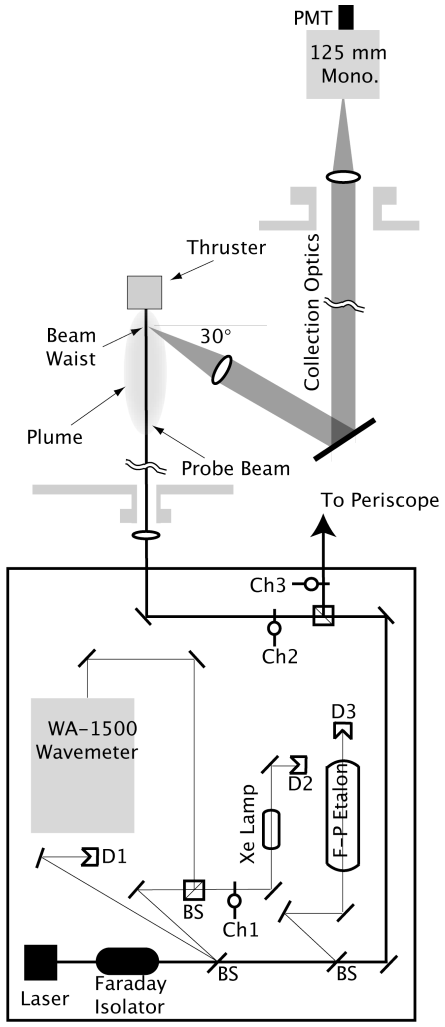


**Figure 3. Top view diagram of the laser optical train and collection optics. Note that the radial probe beam periscope and focusing optics are not shown.**

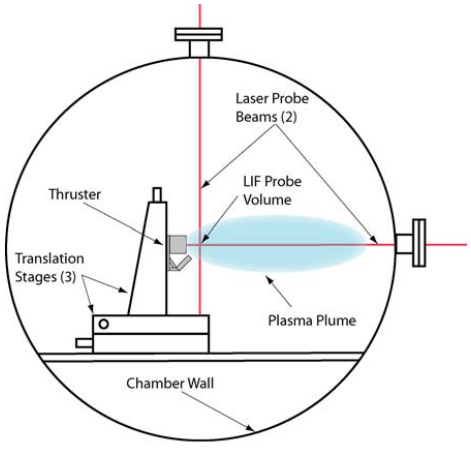


**Figure 4. Side view diagram of thruster within AFRL chamber 6. Also shown are the translation stages and the laser probe beams. Note that the fluorescence collection and external optics are not shown.**

spontaneous emission, and $\Omega$ is the solid angle subtended by the collection optics. The uncertainty of the velocity measurements is estimated to be within $\pm 500$ m/s for the most probable values. The repeatability of the peak locations appears to be a fraction of the quoted uncertainty. However, the fluorescence line shapes are often significantly broadened, presumably due to wide velocity distributions caused by plasma fluctuations. The quoted uncertainty should therefore be viewed as the uncertainty in the determination of the peak of the fluorescence line shape. Measurements confirm that this combination of apparatus and laser power are well within the linear fluorescence regime.

## III. Results and Discussion

As described above, two operating conditions are presented in this study: a high current mode, for which the anode discharge current is oscillatory; and a low current mode for which the anode discharge is quiescent. The ion velocities presented in this study represent most probable (or peak) values calculated using the shift relative to the stationary reference in the LIF excitation profile, as shown in Fig. 5. At this point, velocity distribution functions are not extracted from the measured unsaturated lineshapes because we cannot say with certainty that the spectral lines are not significantly affected by Zeeman splitting. The most probable ion velocities are therefore used to show trends in the data, and in some cases to estimate the electric field from corresponding changes in kinetic energy.

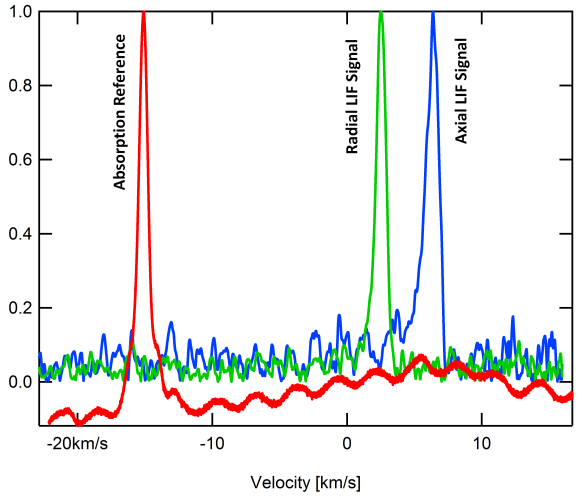


**Figure 5. Example of LIF and absorption traces taken at R = 4 mm and Z = 4 mm.**

The most probable ion velocities for both the high and low current conditions are presented as contour plots in Figs. 6 to 11. In each case, the magnetic field profile and location of the LIF measurements are overlaid. The magnetic field lines shown are for visualization of the field direction, and their spacing should not be taken as indicative of the varying magnetic field strengths. The contour plot was achieved by forming a rectangular grid with 4 mm spacing in the axial and radial directions, and using a weighted average dependent on the distance between points to interpolate the data. Therefore, the contours directly surrounding the data points can be considered to be most accurate, while those not surrounding data points (i.e. in the hollow center of the plume) are meant only to continue the trends seen in the measurements.

## A. High Current Mode

Figs. 6 through 8 show contour plots of the most probable xenon ion velocities measured for the high current mode of operation.

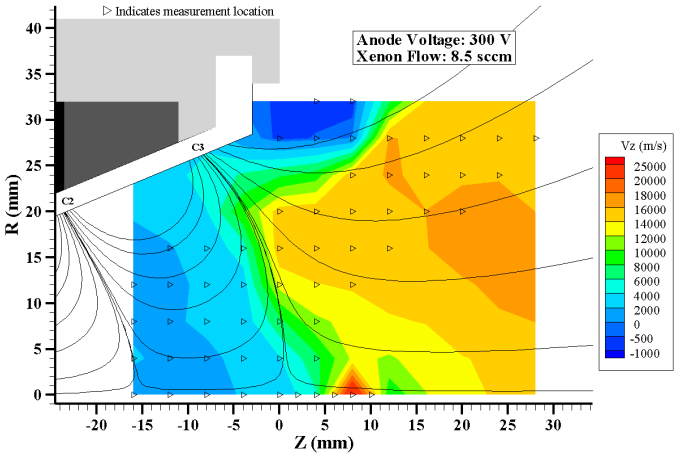


**Figure 6. Contour plot of most probable axial ion velocities for the high current operating condition, including magnetic field line overlay.**

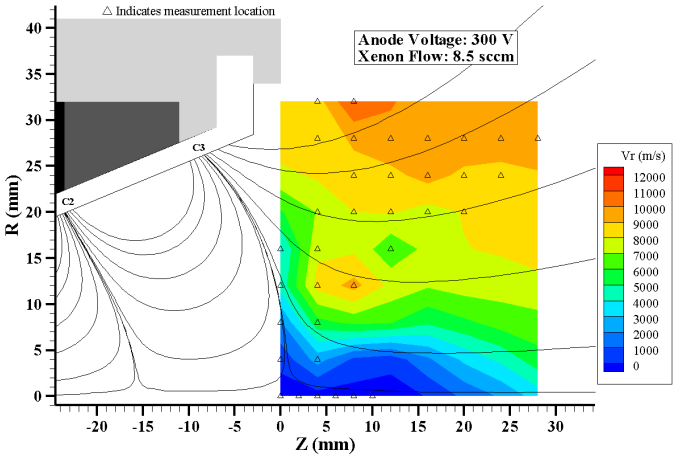


**Figure 7. Contour plot of most probable radial ion velocities for the high current operating condition, including magnetic field line overlay.**

We see from Fig. 6 that the majority of the high speed ions ($v > 15$ km/s) reside in the plume outside of the thruster, just beyond the third magnetic cusp. Rapid axial acceleration appears to occur perpendicular to the magnetic separatrix of this most downstream cusp. It is interesting to note that some acceleration occurs upstream of this point, most probably in the vicinity of the second cusp, although measurements were not able to be taken far enough upstream to resolve this region of the flow. It is also apparent that at any axial location, the ions are generally slowest near the centerline and faster at approximately 2/3 of the exit radius, with lines of constant velocity following allong the separatricies of the last two cusps.

The contour plot of the radial velocities indicates that the highest radial velocities occur in the jet region of the plume at a radius of 25 mm or more off-axis. In this jet region, the radial velocities are of comparable magnitude to the axial velocities (e.g. around 16,000 m/s axial, 10,000 m/s radial), which is indicative of the highly divergent nature of cusped field thrusters. Along the centerline of the thruster, there is little to

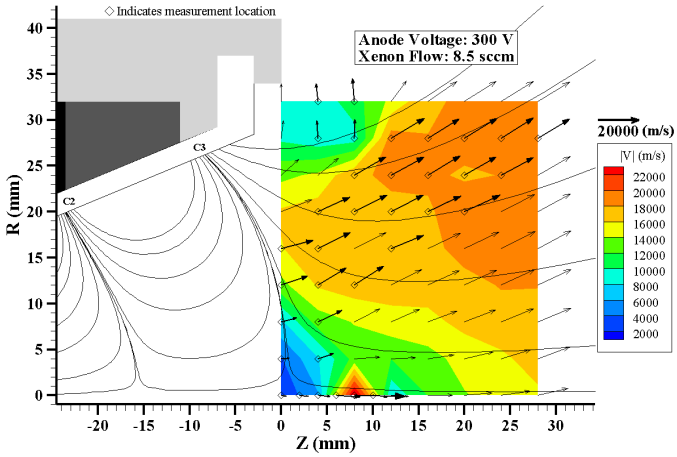


**Figure 8. Contour plot of the magnitude of the total most probable ion velocities for the high current operating condition, including magnetic field line overlay. Arrows indicate the direction of the velocities.**

no radial velocity. This is in contrast to the CHT-30 thruster in which there appears to be a convergence of the velocity field towards the axis.[7,8,14] This also differs from the ion velocity fields seen in many traditional Hall thrusters[31] where there is a mixing region in front of the nosecone where ions from opposite sides of the annular thruster channel cross paths due to their inward-directed radial velocities originating along the channel centerline.

Fig. 8 provides a contour plot of the overall magnitude of the ion velocity. Superimposed in this figure are vectors pointing along the local ion flow direction, the lengths of which are equal to the local ion speed. We see that close to the separatrix of the third cusp, the ion acceleration appears to be normal to the field line, suggesting that the field lines near the cusps represent lines of low parallel resistivity. This correlation between the direction of ion velocity and the direction normal to the field lines breaks down further downstream of the cusp, and by approximately 15 mm into the plume it appears that the ions begin to follow the divergent magnetic field. While it is tempting to believe that ions may be tied to the magnetic field by the nature of their trajectories, the relatively large ion Larmor radius ($> 0.1$ m) in this region of the flow suggests that the ion trajectories are initially defined by the accelerations experienced further upstream, while still experiencing small corrections by the electrostatic influence of strongly magnetized electrons that are tied to the field lines further downstream of the cusps.

Measurements taken along the Z-axis indicate that for the high current mode, there is a strong acceleration and subsequent deceleration seen between axial locations of 5 and 15 mm. In the present experiments, this is a region of very low signal to noise, and so these data should be interpreted with caution. The ion transport in this region should be re-examined in future studies, with longer scan durations.

## B. Low Current Mode

The low current mode of operation is achieved by lowering the anode flow rate as well as raising the applied anode potential. As mentioned above, the low current mode operated without strong oscillations in the discharge current. The lower flow rate made the discharge visibly less bright than that of the high current mode of operation, indicating that there are fewer xenon atoms occupying excited electronic states. This resulted in fewer positions from which data can be obtained with sufficiently high S/N to make meaningful measurements of velocity.

Figs. 9 and 10 depict contour plots (with measurement locations and magnetic field lines superimposed)

of the most probable axial and radial xenon ion velocities measured for the low current mode of operation, respectively. Fig. 8 gives the magnitude of the total ion velocity, with vectors indicating the direction of the flow. In general, the contour plots of the low current mode of operation show some similar trends to those seen in the high current mode. However, there are several ion velocity field characteristics that distinguish this low current mode from its oscillatory, more diffuse counterpart. For example, an examination of Fig. 9 reveals that there is a more abrupt axial acceleration taking place along the separatrix of the third cusp. Upstream of this separatrix, the ion velocities seem to be very low, suggesting that in the low current mode, less acceleration (if any) takes place near the second cusp. Also, the rapid acceleration and high ion velocities seen along the centerline in Fig. 6 is not apparent in the low current case.

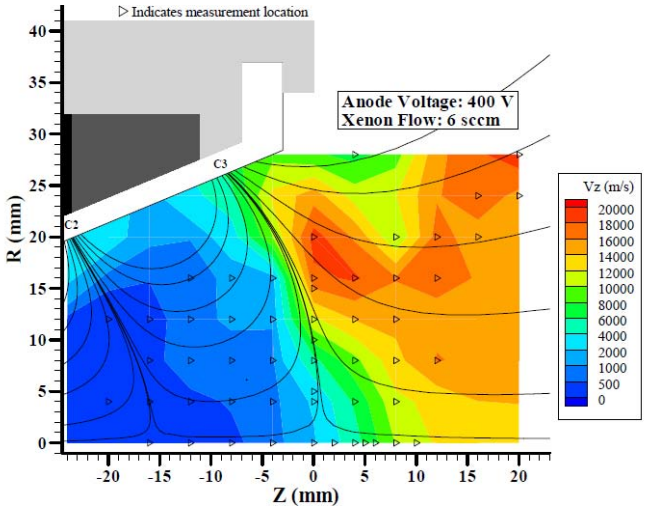


**Figure 9. Contour plot of most probable axial ion velocities for the low current operating condition, including magnetic field line overlay.**

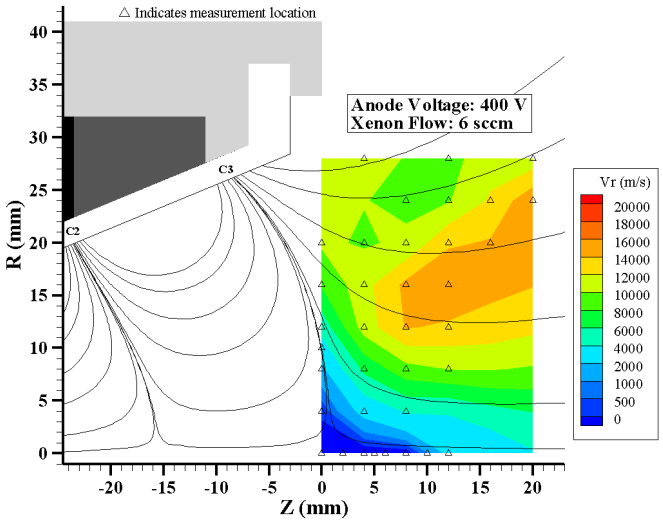


**Figure 10. Contour plot of most probable radial ion velocities for the low current operating condition, including magnetic field line overlay.**

An examination of Fig. 10 reveals that there are strong radial components to the ion velocity as close as 10 mm from the centerline. The development of a strong radial component so close to the axis, results in a much stronger divergence of the ion beam (see Fig. 11), when compared to the flow field for the low current mode

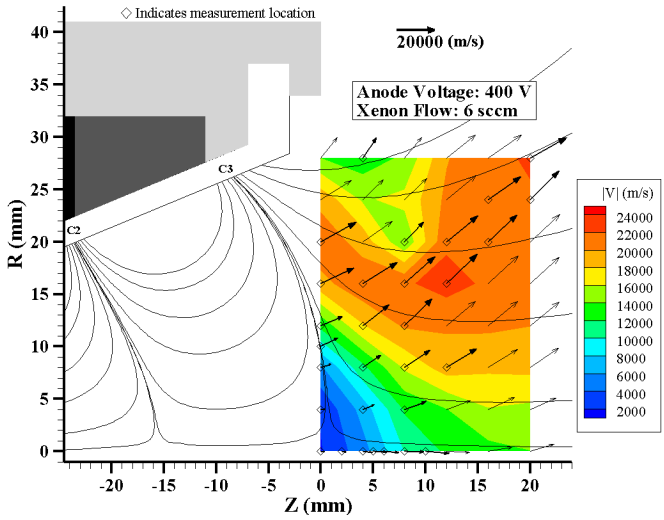


**Figure 11. Contour plot of the magnitude of the total most probable ion velocities for the low current operating condition, including magnetic field line overlay. Arrows indicate the direction of the velocities.**

depicted in Fig. 8. Visually comparing the thruster plumes, it appears that they have similar divergence half angles (between 30° and 40°[21]), however the low current mode shows a distinct, more lumanous jet at this angle, whereas the high current mode is luminous throughout the center of the cone, not appearing as hollow.

The differences in velocity fields presented here must be interpreted with caution, as the LIF measurements are are averaged over time. While the low current mode has a quiescent discharge current, the high current mode exhibits strong low frequency ($\approx$ 3 kHz)[18] discharge current oscillations indicative perhaps of a fluctuation in the position of the ionization zone. Such a fluctuation can partially explain the deeper extension of the acceleration (closer to the second cusp) that is seen in this high current mode, and the lower concentration of ion flux in the conical jet.[21] This behavior would be best resolved with a velocity diagnostic capable of being synchronized to the discharge current oscillations.

### C. Centerline Kinetic Energy and Electric Fields

Fig. 12 depicts the variation in the most probable axial ion kinetic energy along the centerline of the thruster, which we can assume is a probable streamline for ions born along the centerline. Along the centerline, acceleration to a given kinetic energy occurs sooner for the case of the high current mode, but in both cases, acceleration tends to increase rapidly beyond the thruster exit plane. This centerline energy can be used to estimate the electric field, assuming that the ionization takes place upstream of the axial location where the acceleration is seen. Fig. 13 shows the implied axial electric fields corresponding to the data of Fig 12. These data suggest that the vast majority of the potential drop along the centerline of the thruster takes place well beyond the exit plane. It is noteworthy that preliminary emissive probe data taken along the centerline indicates that the region of strong electric field peaks very near the exit plane.[19] While probe measurements must be interpreted with caution as they are inherently intrusive, the discrepancy can also be attributed, at least partially, to the possibility that ionization is more distributed along the axis than what is assumed in generating the data in Fig. 13. However, the sudden acceleration that is defined by the increase in ion velocity at a location of approximately z = 0 mm (exit plane), as depicted by Figs. 6, 9, and 12 is consistent with the location of where the separatrix from the third cusp intersects the thruster centerline, suggesting perhaps that this strong magnetic flux surface forms a barrier to electron transport, defining a resistance to

electron flow and a potential barrier for ion acceleration.

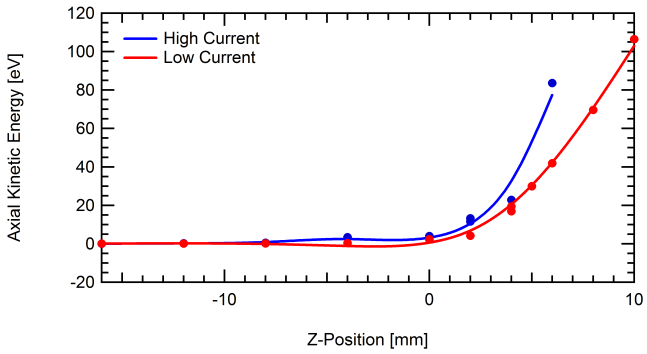


**Figure 12. Axial kinetic energies derived from the most probable axial ion velocities along centerline of thruster plume.**

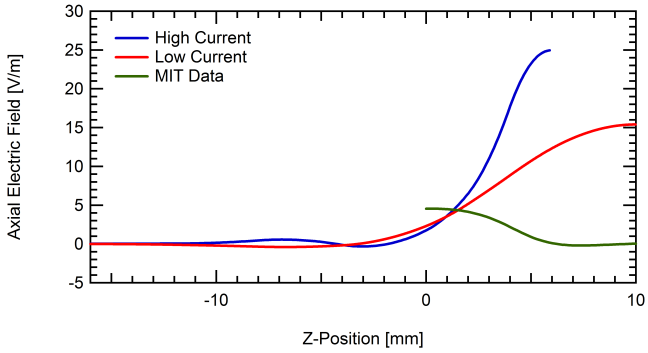


**Figure 13. Axial electric fields derived from most probable kinetic energies along the centerline of the plume. The LIF derived electric fields are compared to the axial electric field derived from emissive probe plasma potential data.**

## IV. Conclusions

Laser induced fluorescence was used to map the most probable ion velocities both inside the thruster channel and in the plume of the MIT developed DCFT. Two operating conditions were examined, including a high current, oscillatory mode, and a low current, quiesent mode. Contour plots of the most probable axial and radial ion velocities revealed several trends, including slower ions appearing inside the thruster channel near the centerline, with the fastest ions appearing after the separatrix formed at the third magnetic cusp. The magnetic field lines of this outermost separatrix appear to form lines of equal potential, with the majority of ion acceleration occurring near the exit plane in the plume of the thruster. Along the centerline of the thruster, the peak acceleration near the exit plane is confirmed by the estimated electric field which showed that the peak potential drop occurs between 5 and 10 mm into the plume. Farther from the exit plane, the ion motion is indicative of ballistic trajectories that are no longer tied to the magnetic field lines.

The low current mode showed a more abrupt axial acceleration at the third cusp separatrix than the high current mode, and had stronger radial components of ion velocity closer to the centerline. These features caused the low current mode of operation to have a more hollow, cone shaped plume with a well contained jet at an angle between 30° and 40°, while the plume of the high current mode was more diffuse. The diffuse plume appears to be related to the oscillatory nature of the high current mode, in that the

regions of ionization and acceleration may oscillate between the second and third cusps. To gain a better understanding of the differences between the high and low current modes, development of a laser-induced fluorescence measurement that is synchronized to the discharge current would be necessary to capture the dynamics of the thruster operation.

## V. Acknowledgments

The authors would like to thank B. Gregory, Lt. A. Campos, and G. Arzonia for their technical support. N. MacDonald and S. Gildea acknowledge the Science Mathematics And Research for Transformation (SMART) scholarship program for support of their research. Research at MIT and Stanford is funded through the Air Force Office of Scientific Research with Dr. M. Birkan as grant monitor.

## References

[1]Goebel, D. M. and Katz, I., *Fundamentals of Electric Propulsion: Ion and Hall Thrusters*, JPL Space and Technology Series, John Wiley & Sons, 2008.

[2]Cappelli, M. A., "The Hall Effect and Rocket Flight," *Physics Today*, Vol. April, April 2009, pp. 76–77.

[3]Kim, V., "Main Physical Features and Processes Determining the Performance of Stationary Plasma Thrusters," *Journal of Propulsion and Power*, Vol. 14, No. 5, 1998, pp. 736–743.

[4]Koch, N., Harmann, H.-P., and Kornfeld, G., "Development & Test Status of the THALES High Efficiency Multistage Plasma (HEMP) Thruster Family," *Proceedings of the 29th International Electric Propulsion Conference*, No. IEPC-2005-297, American Institute of Aeronautics and Astronautics, November 2005.

[5]Koch, N., Harmann, H.-P., and Kornfeld, G., "Status of the THALES High Efficiency Multi Stage Plasma Thruster Development for HEMP-T 3050 and HEMP-T 30250," *Proceedings of the 30th International Electric Propulsion Conference*, No. IEPC-2007-110, September 2007.

[6]Raitses, Y. and Fisch, N. J., "Parametric investigations of a nonconventional Hall thruster," *Physics of Plasmas*, 2001.

[7]Raitses, Y., Smirnov, A., and Fisch, N. J., "Cylindrical Hall Thrusters," *Proceedings of the 37th AIAA Plasmadynamics and Lasers Conference*, No. AIAA-2006-3245, American Institute of Aeronautics and Astronautics, June 2006.

[8]Smirnov, A., Raitses, Y., and Fisch, N. J., "Experimental and Theoretical Studies of Cylindrical Hall Thrusters," *Physics of Plasmas*, Vol. 14, No. 057106, 2007.

[9]Raitses, Y., Smirnov, A., and Fisch, N. J., "Effects of enhanced cathode electron emission on Hall thruster operation," *Physics of Plasmas*, Vol. 16, No. 057106, 2009.

[10]Courtney, D. G. and Martinez-Sanchez, M., "Diverging Cusped-Field Hall Thruster (DCHT)," *Proceedings of the 30th International Electric Propulsion Conference, Florence, Italy*, No. 39, 2007.

[11]Young, C. V., Smith, A. W., and Cappelli, M. A., "Preliminary Characterization of a Diverging Cusped Field (DCF) Thruster," *Proceedings of the 31st International Electric Propulsion Conference*, No. IEPC-2009-166, American Institute of Aeronautics and Astronautics, September 2009.

[12]Bosch, E. and Fleury, G., "Space TWTs Today and their Importance in the Future," *Proceedings of the 22nd AIAA International Communications Satellite Systems Conference & Exhibit 2004*, No. AIAA 2004-3259, May 2004.

[13]Smirnov, A., Raitses, Y., and Fisch, N. J., "The Effect of Magnetic Field on the Performance of Low-Power Cylindrical Hall Thrusters," *Proceedings of the 29th International Electric Propulsion Conference*, No. IEPC-2005-099, Princeton, NJ, 2005.

[14]MacDonald, N. A., Cappelli, M. A., and Hargus Jr., W. A., "Laser-Induced Fluorescence Velocity Measurements of a Low Power Cylindrical Hall Thruster," *Proceedings of the 31st International Electric Propulsion Conference*, 2009.

[15]MacDonald, N. A., Cappelli, M., and W. A. Hargus, J., "Ion Velocity Distribution in a Low-Power Cylindrical Hall Thruster," *Proceedings of the 46th AIAA/ASME/SAE/ASEE Joint Propulsion Conference & Exhibit*, 2010.

[16]Courtney, D. G., Lozanoy, P., and Martinez-Sanchez, M., "Continued Investigation of Diverging Cusped Field Thruster," *Proceedings of the 44th AIAA/ASME/SAE/ASEE Joint Propulsion Conference & Exhibit*, Hartford, CT, 2008.

[17]Matlock, T., Daspit, R., Batishchev, O., Lozano, P., and Martinez-Sanchez, M., "Spectroscopic and Electrostatic Investigation of the Diverging Cusped-Field Thruster," *Proceedings of the 45th AIAA/ASME/SAE/ASEE Joint Propulsion Conference & Exhibit*, No. AIAA 2009-4813, 2009.

[18]Gildea, S. R., Matlock, T. S., Lozano, P., and Martinez-Sanchez, M., "Low Frequency Oscillations in the Diverging Cusped-Field Thruster," *Proceedings of the 46th AIAA/ASME/SAE/ASEE Joint Propulsion Conference & Exhibit*, No. AIAA 2010-7014, Nashville, TN, 2010.

[19]Matlock, T., Gildea, S., Hu, F., Becker, N., P.Lozano, and Martinez-Sanchez, M., "Magnetic Field Effects on the Plume of a Diverging Cusped-Field Thruster," *Proceedings of the 46th AIAA/ASME/SAE/ASEE Joint Propulsion Conference & Exhibit*, No. AIAA 2010-7104, 2010.

[20]Courtney, D. G., *Development and Characterization of a Diverging Cusped Field Thruster and a a Lanthanum Hexaboride Hollow Cathode*, Master's thesis, Massachusettes Institute of Technology, 2008.

[21]Gildea, S. R., Martinez-Sanchez, M., Nakles, M. R., and Hargus Jr., W. A., "Experimentally Characterizing the Plume of a Divergent Cusped-Field Thruster," *Proceedings of the 31th International Electric Propulsion Conference*, Ann Arbor, Michigan, USA, September 2009.

[22]Hansen, J. E. and Persson, W., "Revised Analysis of Singly Ionized Xenon, Xe II," *Physica Scripta*, , No. 4, 1987, pp. 602–643.

[23]Demtroeder, W., *Laser Spectroscopy: Basic Concepts and Instrumentation*, Springer-Verlag, 1996.

[24]Brostrom, L., Kastberg, A., Lidberg, J., and Mannervik, S., "Hyperfine-structure Measurements in Xe II," *Physical Review A*, Vol. 53, No. 1, January 1996, pp. 109–112.

[25]Hargus Jr., W. A. and Cappelli, M. A., "Laser-Induced Fluorescence Measurements of Velocity within a Hall Discharge," *Applied Physics B*, Vol. 72, No. 8, June 2001, pp. 961–969.

[26]Geisen, H., Krumpelmann, T., Neuschafer, D., and Ottinger, C., "Hyperfine Splitting Measurements on the 6265 Angstrom and 6507 Angstrom Lines of Seven Xe Isotopes by LIF on a Beam of Metastable Xe(3P0,3) Atoms," *Physics Letters A*, Vol. 130, No. 4-5, July 1988, pp. 299–309.

[27]Fischer, W., Huhnermann, H., Kromer, G., and Schafer, H. J., "Isotope Shifts in the Atomic Spectrum of Xenon and Nuclear Deformation Effects," *Z. Physik*, Vol. 270, No. 2, January 1974, pp. 113–120.

[28]Manzella, D. H., "Stationary Plasma Thruster Ion Velocity Distribution," *Proceedings of the 30th Joint Propulsion Conference and Exhibit*, No. AIAA-1994-3141, American Institute of Aeronautics and Astronautics, June 1994.

[29]Hargus Jr., W. A. and Nakles, M. R., "Ion Velocity Measurements within the Acceleration Channel of Low-Power Hall Thruster," *IEEE Transactions on Plasma Science*, Vol. 36, No. 5, October 2008, pp. 1989–1997.

[30]Mazouffre, S., Gawron, D., Kulaev, V., and Sadehgi, N., "Xe+ Ion Transport in the Crossed-Field Discharge of a 5-kW-Class Hall Effect Thruster," *IEEE Transactions on Plasma Science*, Vol. 36, No. 5, October 2008, pp. 1967–1976.

[31]Hargus Jr., W. A. and Charles, C. S., "Near Exit Plane Velocity Field of a 200-Watt Hall Thruster," *Journal of Propulsion and Power*, Vol. 24, No. 1, 2008, pp. 127–133.

[32]Miller, M. H. and Roig, R. A., "Transition Probabilities of Xe I and Xe II," *Physical Review A*, Vol. 8, No. 1, July 1973, pp. 480–486.

[33]Moore, C. E., *Atomic Energy Levels*, Vol. II, National Bureau of Standards, 1958.

[34]Eckbreth, A. C., *Laser Diagnostics for Combustion Temperature and Species (2nd ed.)*, Gordon and Breach Publishers, 1996.